Filter Flexibility in a Mammalian K Channel: Models and Simulations of Kir6.2 Mutants

Charlotte E. Capener,* Peter Proks,[†‡] Frances M. Ashcroft,[†] and Mark S. P. Sansom*
*Laboratory of Molecular Biophysics, Department of Biochemistry, Rex Richards Building, University of Oxford, South Parks Road, Oxford, OX1 3QU, United Kingdom; [†]University Laboratory of Physiology, University of Oxford, Parks Road, Oxford, OX1 3PT, United Kingdom; and [‡]Institute of Molecular Physiology and Genetics, Slovak Academy of Sciences, 83334 Bratislava, Slovakia

ABSTRACT The single-channel conductance varies significantly between different members of the inward rectifier (Kir) family of potassium channels. Mutations at three sites in Kir6.2 have been shown to produce channels with reduced single-channel conductance, the largest reduction (to 40% of wild-type) being for V127T. We have used homology modeling (based on a KcsA template) combined with molecular dynamics simulations in a phosphatidycholine bilayer to explore whether changes in structural dynamics of the filter were induced by three such mutations: V127T, M137C, and G135F. Overall, 12 simulations of Kir6.2 models, corresponding to a total simulation time of 27 ns, have been performed. In these simulations we focused on distortions of the selectivity filter, and on the presence/absence of water molecules lying behind the filter, which form interactions with the filter and the remainder of the protein. Relative to the wild-type simulation, the V127T mutant showed significant distortion of the filter such that ~50% of the simulation time was spent in a closed conformation. While in this conformation, translocation of K^+ ions between sites S1 and S2 was blocked. The distorted filter conformation resembles that of the bacterial channel KcsA when crystallized in the presence of a low [K^+]. This suggests filter distortion may be a possible general model for determining the conductance of K channels.

INTRODUCTION

Potassium channels are a ubiquitous family of integral membrane proteins that form K-selective transmembrane (TM) pores (Hille, 2001). There are three main structural classes of mammalian K channels: 1), voltage-gated (Kv) potassium channels; 2), inwardly rectifying K channels (Kirs); and 3), TWIK channels (Biggin et al., 2000). The simplest transmembrane topology is that exemplified by the bacterial K channel KcsA (Doyle et al., 1998; Zhou et al., 2001), which is a tetramer of four identical subunits, each consisting of two TM α-helices linked by a re-entrant P-helix containing the selectivity filter. This topology is also shared by the Kir channels (Reimann and Ashcroft, 1999), and by MthK, a bacterial Ca-activated K channel whose structure has recently been determined (Jiang et al., 2002a). Members of the Kir family, however, also have extensive cytoplasmic domains N- and C-terminal to the transmembrane domains.

Kir channels have two main physiological roles: they regulate cell excitability by stabilizing the membrane potential close to the K-equilibrium potential, and they are involved in K-transport across membranes (Reimann and Ashcroft, 1999). For example, cardiac electrical activity is modulated by Kir3.1/Kir3.4 channels, and Kir6.2 is involved in insulin release from pancreatic β-cells. Kir6.2 is unusual in that it co-assembles with a regulatory subunit, the sulphonylurea receptor, to form an octameric ATP-sensitive potassium (K_{ATP}) channel. This channel is strongly selective for external K, with a permeability ratio (P_{Na}/P_K) of 0.007, but discriminates less strongly against internal Na^+ (P_{Na}/P_K = 0.39) (Ashcroft et al., 1989). In the absence of an x-ray structure for Kir6.2, a homology model based on the structure of KcsA has been generated and studied by molecular dynamics (MD) simulation (Capener et al., 2000; Capener and Sansom, 2002).

There has been some debate as to whether or not Kir channels share a common pore structure with KcsA (Minor et al., 1999; Kubo and Murata, 2001). Although KcsA shows considerable sequence similarity with the members of the Kv family, that with Kir channels is quite low (30% in the pore region and 15% overall). There are also some apparent incompatibilities between the dimensions of the inner pore obtained from the x-ray structure of KcsA and that estimated from the results of stoichiometric covalent modification (Lu et al., 1999) or mutagenesis (Thompson et al., 2000). In addition, Minor et al. (1999) have proposed a different packing arrangement for the transmembrane helices of Kir2.1 to that found for KcsA. However, a homology model of Kir6.2, built using KcsA as a template (Capener et al., 2000), behaves stably in multinanosecond simulations (Capener and Sansom, 2002) and recent sequence alignments of bacterial Kir channel homologs (Durell and Guy, 2001) support the proposed homology between KcsA and Kir6.2 underlying this model.

The single-channel conductance is strikingly different between different Kir channels. The mean conductance of Kir6.2/sulphonylurea receptor channels in symmetrical 140 mM K solution was ~70 pS (Proks et al., 2001), much higher than that of Kir1.1 (38 pS) or Kir2.1 (29 pS) channels under the same conditions (Choe et al., 2000). Within the pore loop region of these channels, their amino acid

Submitted August 9, 2002, and accepted for publication December 4, 2002.

Address reprint requests to Mark S. P. Sansom, Tel.: +44-1865-275371; Fax: +44-1865-275182; E-mail: mark@biop.ox.ac.uk.

0006-3495/03/04/2345/12 $2.00

sequences differ by only four residues (Fig. 1 *A*). Mutations at three of these sites in Kir6.2 produced channels with reduced single-channel conductance: 38 pS for V127T (40% of the wild-type conductance), 50 pS for M137C (70%), and 62 pS for G135F (90%) (Proks et al., 2001). At least in the case of the V127T mutation, these changes in single-channel conductance were not accompanied by a change in the relative permeability to intracellular Na. Despite their marked effects on conductance, none of these mutations lie within the selectivity filter: G135F and M137C lie at the top (i.e., the extracellular end) of the filter, whereas V127T is located at the back of the lower part of the filter. Thus they must mediate their effects indirectly. Because the side chains of these residues, particularly of V127, lie close to the back of the selectivity filter, we were interested to determine whether changes in structural dynamics of the filter were induced by these mutations.

We have previously demonstrated that nanosecond dynamics of the selectivity filter in simulations are dependent on the nature of the ion present, but are largely unaffected by other aspects of simulation setup (Capener and Sansom, 2002). In this paper, we employ simulations to explore the interplay between mutations in the pore loop of Kir6.2 and the presence of water molecules that form part of the selectivity filter. Our results suggest that local changes in channel conformation may explain the changes in single-channel conductance produced by these mutations.

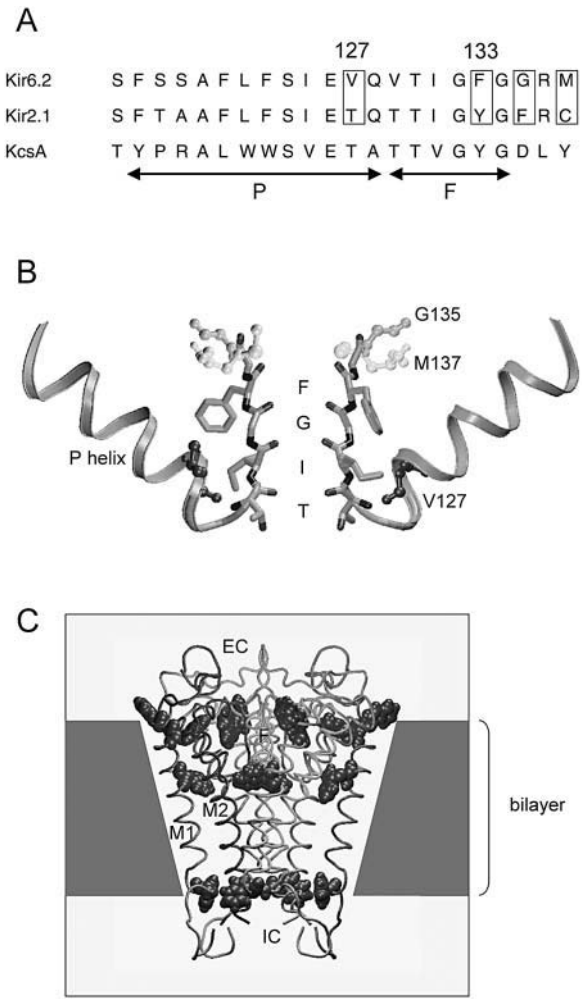

FIGURE 1 (*A*) Sequence alignment of the pore helix (*P*) and filter (*F*) regions for Kir2.1, Kir6.2, and KcsA. The residues for which mutant models have been constructed (see text) are boxed, as is the Y-to-F difference in the GYG motif. Numbering is relative to the Kir6.2 sequence. (*B*) Pore region of the Kir6.2 model (two subunits out of four are shown). The residues which have been mutated (V127, G135, and M137) are shown in ball-and-stick format. (*C*) The Kir6.2 channel model (all four subunits) is shown along with the approximate location of the lipid bilayer. Aromatic side chains used to judge the location of the transmembrane region are shown in space-filling format.

METHODS

Modeling

Homology modeling of the wild-type (WT) channel was performed using Modeller v4 (Sali and Blundell, 1993) as described previously (Capener et al., 2000). Briefly, an ensemble of 25 models was generated with fourfold symmetry restraints and with secondary structure restraints corresponding to secondary structure elements in KcsA. The template structure was the 3.2-Å resolution structure of KcsA (PDB code 1BL8; Doyle et al., 1998). Five top models from the ensemble were selected on the basis of best fit to the restraints and an assessment of stereochemical quality was also performed (Morris et al., 1992) to select an overall best model. Side-chain ionization states were adjusted to match the results of pK_A calculations, performed as described in Adcock et al. (1998), using UHBD (Davis et al., 1991) to calculate free energy differences between ionized and unionized side chains of the protein. This resulted in an overall charge for the protein tetramer of $-14e$. Most of the side chains remained in their default ionization states. Close to the selectivity filter one of the four E126 side chains was protonated and one of the four K136 side chains was deprotonated.

Homology modeling of the mutants was performed using Modeller v6 (see http://guitar.rockefeller.edu/modeller/modeller.html). For each mutant the Kir6.2 WT model (Capener et al., 2000) was used as the template structure. The required mutation was defined in the sequence alignment file which is input into the Modeller program. The number of models generated per mutant was set to 5 and the maximum deviation between template and target to 4 Å. Fourfold symmetry restraints were defined for the mutant models as for the WT, and residues H70-A94 (M1), S116-Q128 (P-helix), and L14487-M169 (M2) were restrained to be α-helical.

Simulations

Simulations were performed in an explicit phospholipid bilayer. The mutant models were placed into a palmitoyloleoyl phosphatidycholine (POPC) bilayer which had been pre-equilibrated around the WT model and energy-minimized as described in Capener et al. (2000) and Capener and Sansom (2002). Filter waters and ions were placed by fitting backbone and Cβ atoms of the KcsA filter (PDB 1K4C and 1K4D) onto the Kir models and transferring across the ion and water coordinates. The system was energy-minimized again at this stage. The central cavity contained one K^+ ion and 20 water molecules. The latter number was decided by calculation of the approximate volume of the cavity (by integrating the pore radius profile) and assuming a water density in the cavity the same as that of bulk water (Capener and Sansom, 2002). The systems were rendered electroneutral by addition of 11 K^+ counterions at random locations in the bulk-water regions either side of the bilayer. The simulation box was $\sim 9 \times 9 \times 8.5$ nm^3. The

number of POPC molecules was 235 and of waters was 11729, resulting in system sizes of ~50,000 atoms.

Molecular dynamics simulations used Gromacs2.0 (www.gromacs.org) as described in detail in Capener et al. (2000) and Capener and Sansom (2002). The LINCS algorithm (Hess et al., 1997) was used to constrain bond lengths. Simulations were performed under NPT conditions, i.e., using isotropic pressure coupling. Water, lipid, and protein were coupled separately to a temperature bath (Berendsen et al., 1984) at 300 K with a coupling constant of $\tau_T = 0.1$ ps. Lipid parameters were as in previous studies of lipid bilayers (Berger et al., 1997; Marrink et al., 1998) and membrane proteins (Tieleman et al., 1999; Shrivastava and Sansom, 2000). These lipid parameters give acceptable reproduction of the experimental properties of a DPPC bilayer. The water model used was SPC (Hermans et al., 1984), which behaves reasonably in bilayer/water simulations (Tieleman and Berendsen, 1996). K^+ parameters were as in Straatsma and Berendsen (1988). The timestep was 2 fs. Long-range interactions were treated using a twin-range cutoff set to 10 Å for van der Waals interactions and 17 Å for electrostatic interactions.

Each system was subjected to a 200-ps equilibration simulation during which non-H-atoms of the protein and the filter potassium ions were restrained. For simulations with waters behind the selectivity filter (see below) the O-atoms of these water molecules were also restrained. The restraining force constant was 1000 kJ mol^{-1} nm^{-2} in the x, y, and z directions. For each system, the equilibration period was followed by 2 ns of unrestrained (production) MD during which coordinates were saved every 1 ps for analysis.

Analysis

Analysis of simulation results was carried out using Gromacs routines and/or local scripts. Pore radius profiles were evaluated using HOLE (Smart et al., 1993, 1996). Molecular graphics manipulations were via VMD (Humphrey et al., 1996) and Raster3D (Merritt and Bacon, 1997).

RESULTS

Mutants and models

The main aim of this study was to explore possible changes in the conformational dynamics of the filter region of Kir6.2 associated with mutations which are known to reduce the single-channel conductance. Three mutant Kir6.2 models have been constructed—V127T, G135F, and M137C—based on a structural model of the transmembrane domains of Kir6.2 (Capener et al., 2000). Examination of the model of the filter region (Fig. 1 *B*) reveals that V127 is at the bottom of the filter, where the filter per se is packed against the C-terminus of the corresponding P-helix. In contrast, the other two mutation sites (G135 and M137) are at the top of the filter. As the top of the filter is next to the loop that joins the filter to the M2-helix, and given that simulations of both Kir6.2 (Capener et al., 2000; Capener and Sansom, 2002) and KcsA (Shrivastava and Sansom, 2000; Bernèche and Roux, 2000) suggest that this loop is relatively mobile, one might expect mutations in a more inherently flexible region to have a smaller effect than those deeper within the protein structure. This is indeed the case, with the V127T mutation having the largest effect on single-channel conductance (reduced to 40% of the conductance of the WT channel).

The models of the WT channel and of the three mutant channels were used as the starting points for multinanosecond MD simulations, to explore possible changes in filter structure and dynamics. These simulations were performed for the models of the channel domain embedded within a POPC bilayer (Fig. 1 *C*). The location of the protein within the bilayer was guided by the presence of two bands of aromatic side chains in the Kir6.2 model. Such bands of aromatic side chains have been seen in a number of membrane proteins and seem to correlate with the location of the lipid headgroup region of the bilayer (Schiffer et al., 1992; Yau et al., 1998; Killian and von Heijne, 2000).

Simulations

Previous simulations, both of Kir6.2 (Capener et al., 2000; Capener and Sansom, 2002) and of KcsA (Shrivastava and Sansom, 2000), suggest that K^+ ions must be present within the filter to prevent large distortions of this region. There are five main sites within K channel filters, referred to as S0 (at the extracellular end of the filter) to S4 (at the cavity end of the filter). A combination of structural, physiological, and simulation results (Morais-Cabral et al., 2001; Bernèche and Roux, 2001) suggests that two states of KcsA are of nearly equal thermodynamic stability, one with K^+ ions in sites S1 and S3, and one with K^+ ions in sites S2 and S4. All of our simulations started with one of these configurations, namely S1 occupied by a K^+ ion, S2 by a water molecule, and S3 by a K^+ ion. Following the nomenclature of Åqvist and Luzhkov (2000), we refer to this as the 01010 configuration, where 0 indicates a water molecule (at sites S0, S2, and S4) and 1 indicates a K^+ ion (at sites S1 and S3).

From the recent 2-Å resolution structures of KcsA, it is evident that a number of water molecules form part of the filter structure, sitting behind the selectivity filter and bridging between the filter and the remainder of the protein (Zhou et al., 2001). Both the structural studies and recent simulation data (Domene and Sansom, unpublished data) suggest these water molecules play an important role in the conformation and dynamics of the filter. For example, comparison of the x-ray structures of KcsA in the presence of high $[K^+]$ or low $[K^+]$ reveals one water/subunit behind the filter in the high $[K^+]$ structure whereas three waters/subunit are behind the filter in the low $[K^+]$ structure, forming additional H-bonds between the filter and the rest of the protein. To explore the influence of water molecules near the filter on the simulation results, we constructed initial models (for both the WT and mutant channels) with either zero, one or three water molecules per subunit behind the filter. Water molecules were placed behind the selectivity filter corresponding to their locations within the KcsA x-ray structures: one water per subunit was positioned as for the KcsA structure solved under high K^+ (200 mM) conditions (PDB 1K4C); and three waters per subunit were positioned as for the low K^+ (3 mM) KcsA structure (PDB 1K4D) (see Fig. 2).

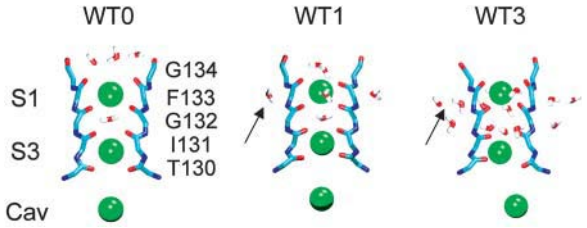

FIGURE 2 Initial filter configurations (two subunits only shown) for simulations WT0, WT1, and WT3. K^+ ions (*green spheres*) are present at S1, S3, and in the cavity. Water molecules within and behind the filter are shown (in *red*/*white*) as indicated by the arrows.

Thus a total of 12 simulations were performed (Table 1), corresponding to the WT and the three mutant channels, each with zero, one, or three waters/subunit behind the filter.

Structural stability and drift

To check for global changes in protein conformation as a result of the mutations and/or simulation setup (i.e., addition of water molecules behind the filter) we examined the overall drift of the structure in each simulation, measured as the Cα RMSD relative to the starting model for a simulation. This was measured for the transmembrane core (i.e., the M1 and M2 helices plus the P-helix and filter regions) so as to exclude effects of structural drift of the mobile surface loops (i.e., the M1-P loop and the filter-M2 loop) and terminal tails. Comparison between the different simulations (Table 1) suggests that the overall RMSD is a little higher for the mutant simulations than for the WT simulation, and is highest for the V127T mutant simulations. However, analysis of RMSDs as a function of time (Fig. 3) suggests one should not over-interpret these relatively small differences. From these graphs it is evident that the major component of the RMSD from the initial structure is over within ~0.5 ns. It is difficult to dissect out such an RMSD into components from structural drift versus from fluctuations around an equilibrium structure. The WT0 simulation was extended to 5 ns total but no further significant increase in core Cα RMSD was seen (Table 1). We are therefore reasonably confident that a 2-ns simulation period is sufficient to reveal significant local conformation changes resulting from the mutations.

We also calculated Cα RMSD values for just the pore helix and filter regions (P + F; Table 1) to assess the more local disturbances around the selectivity filter region due to the mutations. In general, the RMSDs are smaller than for the TM core as a whole, but suggest the same general pattern. In particular, only the V127T mutation shows any significant change in RMSD value, reaching an average value of ~0.20 nm for the three V127T simulations compared with ~0.15 nm for the WT simulations.

TABLE 1 Simulations performed

Simulation	Model	Waters	Duration (ns)	Core Cα RMSD(nm)	P + F region Cα RMSD (nm)
WT0	Wild-type	0	2*	0.18	0.16
WT1	Wild-type	1	2	0.16	0.13
WT3	Wild-type	3	2	0.16	0.15
VT0	V127T	0	2	0.24	0.17
VT1	V127T	1	2	0.17	0.18
VT3	V127T	3	2	0.28	0.24
GF0	G135F	0	2	0.21	0.17
GF1	G135F	1	2	0.24	0.15
GF3	G135F	3	2	0.24	0.15
MC0	M137C	0	2	0.19	0.13
MC1	M137C	1	2	0.18	0.15
MC3	M137C	3	2	0.24	0.18

*The WT0 simulation was extended to 5 ns to check for any further significant structural drift after 2 ns. We therefore report RMSDs for the last 0.5 ns of the 2-ns and of the 5-ns simulation period.

Summary of simulations performed, defining the nomenclature used in the text. The number of waters per subunit positioned behind the selectivity filter in the initial setup of the systems was: 0 = no waters behind filter; 1 = a single water per subunit behind filter, as in the high [K^+] structure of KcsA (PDB code 1K4C); and 3 = three waters per subunit behind the filter, as in the low [K^+] structure of KcsA (PDB code 1K4D). RMSD values are calculated over the final 500 ps of each simulation for the Cα atoms of the core TM region (i.e., M1 and M2 helices plus P + F region (the latter defined as residues T116 to G135).

Distortions of the filter

Visualization of the filter region at the end of 2 ns for each simulation (Fig. 4) provides a clear first indication of specific differences in filter conformation generated by the different simulations. Over the course of the WT simulations the filter conformation is largely conserved, with some limited motion of residue G134 at the extracellular mouth of the filter. In contrast the V127T (VT) simulations show considerable distortion, with flipping of the I131 carbonyls in VT0 and VT1, and some much larger deformation in VT3 where

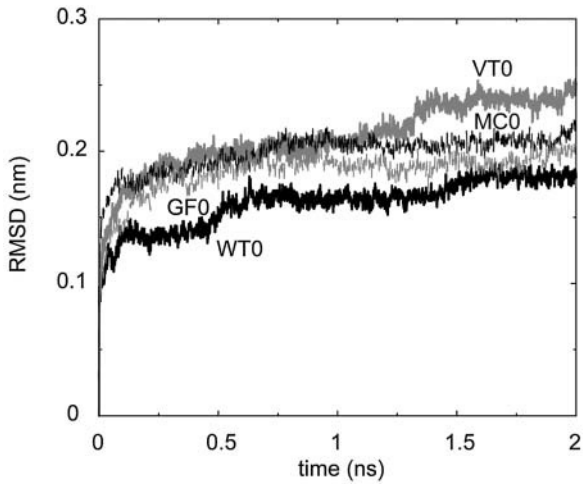

FIGURE 3 Cα RMSD of the TM region (i.e., the M1 helix, the P-helix, and filter, and the M2-helix) versus time for the WT0 (*solid*, *black*), VT0 (*solid*, *gray*), GF0 (*broken*, *gray*), and MC0 (*broken*, *black*) simulations.

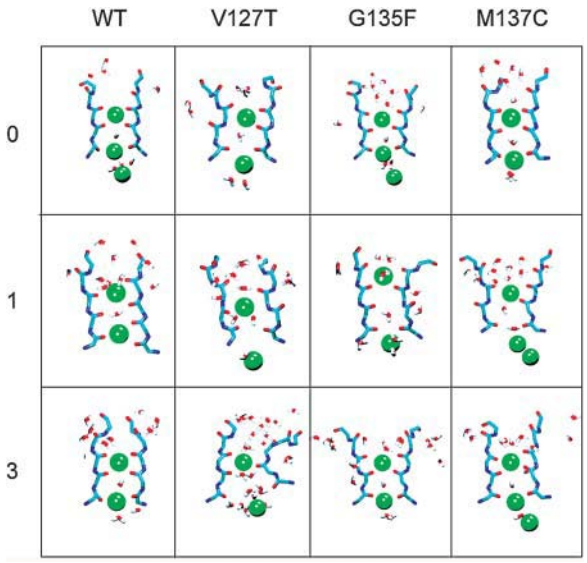

FIGURE 4 Final (i.e., $t = 2$ ns) filter configurations (only two subunits shown), the WT simulations (with 0, 1, and 3 waters per subunit behind the filter—see Table 1 and text), for the V127T mutant simulations, for the G135F mutant simulations, and for the M137C mutant simulations.

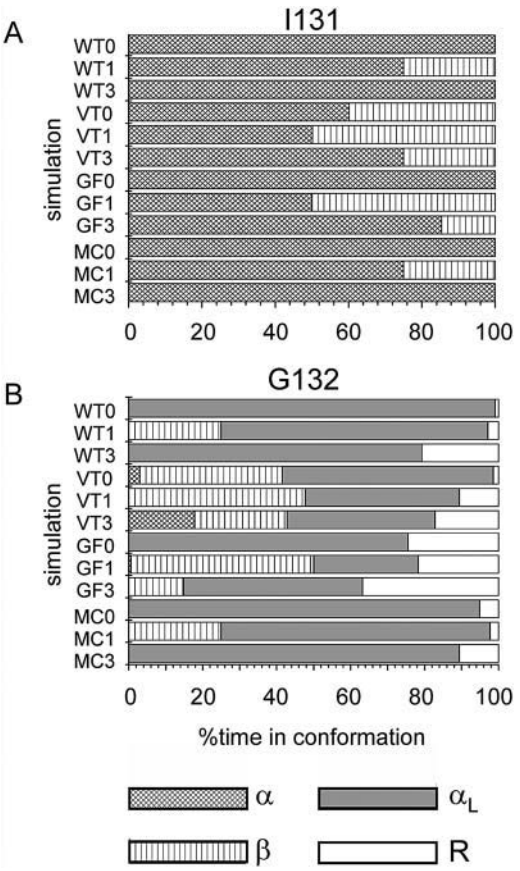

FIGURE 5 Summary of the conformations adopted by (*A*) residue I131 and (*B*) residue G132 in all simulations as a percentage of time, averaged over the period 0.5–2.0 ns of each simulation. α-Helix (cross-hatch) is defined as $0° \geq \Phi \geq -180°$ and $+30° \geq \Psi \geq -130°$; β-strand (*vertical stripes*) is defined as $0° \geq \Phi \geq -180°$ and ($+180° \geq \Psi \geq +30°$ or $-130° \geq \Psi \geq -180°$); left-handed α-helix (*gray*) is defined as $+110° \geq \Phi \geq 0°$ and $+120° \geq \Psi \geq -30°$; all other regions are defined as random coil (*empty*). Note that these regions correspond to rectangles in the Ramachandran plot that approximate the secondary structure regions defined in e.g., Procheck (Morris et al., 1992).

several water molecules have entered the filter from both the extracellular mouth and from the interior aqueous cavity. The behavior of the G135F (GF) and M137C (MC) simulations appears intermediate between that of WT and VT. There is some carbonyl flipping seen in the GF1 and MC1 simulations, and also some other minor deviations from initial structure.

Filter flexibility

To quantify the differences observed in the behavior of the selectivity filter, we determined the backbone torsion angles of the filter residues as a function of time for each of the simulations. To simplify comparisons we defined four broad regions of (Φ,Ψ) space corresponding to four possible conformations of each residue, namely α, β, α_L, and random coil (see Fig. 5 legend for details). We then calculated the percentage of the total simulation time that a given residue spends in each of these conformations. The results of these calculations are shown in Fig. 5 for residues I131 and G132, which showed consistent differences in conformation between the WT and mutant simulations. Looking first at the WT0 simulation, we see that I131 spends all of its time in the α-conformation, as in the starting model, and that G132 is found in the α_L conformation (again as in the starting model) for 98% of the time. This combination (I131α, G132α_L) corresponds to a structure in which all carbonyls are directed toward the pore. This contrasts with the picture for VT0. Here, the (I131α, G132α_L) combination occurs for only ~50% of the simulation time. The remainder is spent in a predominantly (I131β, G132β) combination which corresponds to the Ile carbonyls being oriented away from the pore. These two distinct structures have also been observed in simulations of KcsA (Bernèche and Roux, 2000; Shrivastava et al., 2002; Sansom et al., 2002) and are related to the filter structure of KcsA seen in crystals grown in the presence of low [K^+] (see below).

From the analysis in Fig. 5 we can also see that neither GF0 nor MC0 exhibits this (I131β, G132β) combination. The V127T mutation is the only case where this structure occurs significantly when there are no waters initially present behind the selectivity filter. The presence of a single water molecule behind the filter is sufficient to allow this additional conformational space to also be explored by the other mutants and the WT model, with the (I131β, G132β) combination structure occurring for ~25% of the time in the WT1 simulation compared with ~50% for VT1, ~50% for GF1, and ~25% for MC1. Thus both the mutations and the presence of the waters influence the accessible conformational

space for the filter and therefore the observed structures. The presence of three waters per subunit also appears to allow this structure to occur.

It is of interest to examine the timescale of these changes in filter conformation, as exemplified by the simulation VT0 (Fig. 6). Several features are visible. Firstly, the major conformational changes occur in the two opposite subunits of the tetramer. Secondly, they occur in a concerted fashion in all four subunits, with the first transition at ~0.2 ns and the second transition at ~1.3 ns. Thus, the filter switches conformation on a timescale of ~1 ns. This is somewhat faster than the mean timescale of ion permeation for Kir6.2 (~20 ns at 100 mV). Thus one may expect that over a single-channel opening the filter will have plenty of time to sample available conformations (see below). Of course, if the timescale of conformational changes is ~1 ns, then 2-ns simulations do not provide very good sampling. However, by combining subunits and simulations it may be possible to obtain an (approximate) average picture. On this basis, the average percentage time the WT channel model (for all three simulations) spent in the initial (i.e., undistorted) filter conformation for I131 and G132 is ~88%, whereas, for the V127T model, the corresponding average is ~54%.

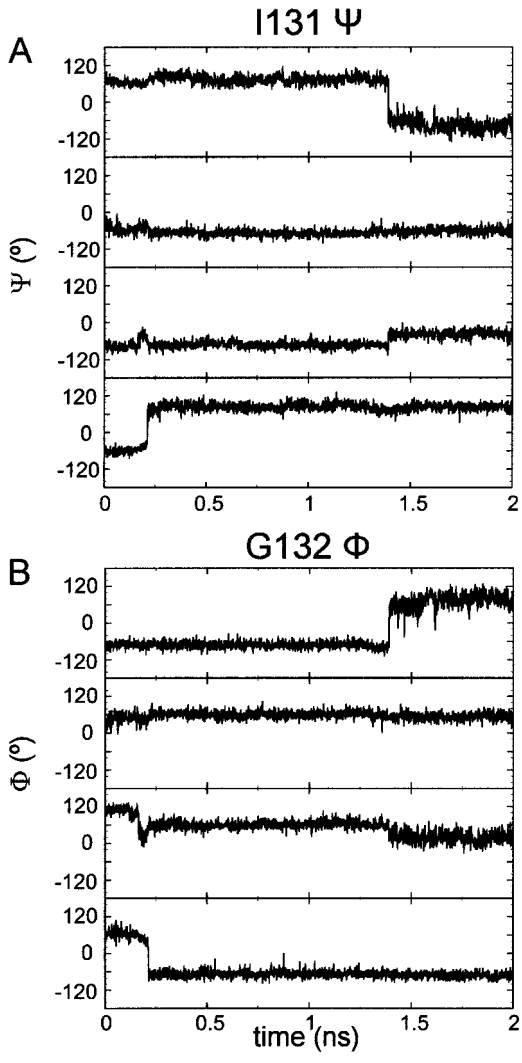

FIGURE 6 Backbone torsion angles versus time: (*A*) I131 Ψ and (*B*) G132 Φ angles, for simulation VT0. The four lines in each graph correspond to the four subunits.

Comparison with KcsA structures

It is valuable to compare the WT and mutant models in these simulations with the structures of KcsA in the presence of high and low concentrations of K^+ ions. In doing so, we recall the proposal that the low [K^+] conformation of the KcsA filter has been suggested to correspond to that which generates fast closures during bursts of channel activity (Zhou et al., 2001). In Fig. 7 we compare the filter conformations of the WT0 and VT0 simulation systems at $t =$ 1 ns with the filter conformations in the two KcsA structures. For the WT0 simulation it is evident that even though the K^+ ion configuration has switched from 01010 to 00101 (see below) the filter has not undergone any major distortion. In particular, the carbonyl oxygens are still all directed toward the center of the pore. In contrast, in the VT0 simulation the ions remain in the same sites as in the WT model (see below) but the filter has distorted somewhat. In partic-

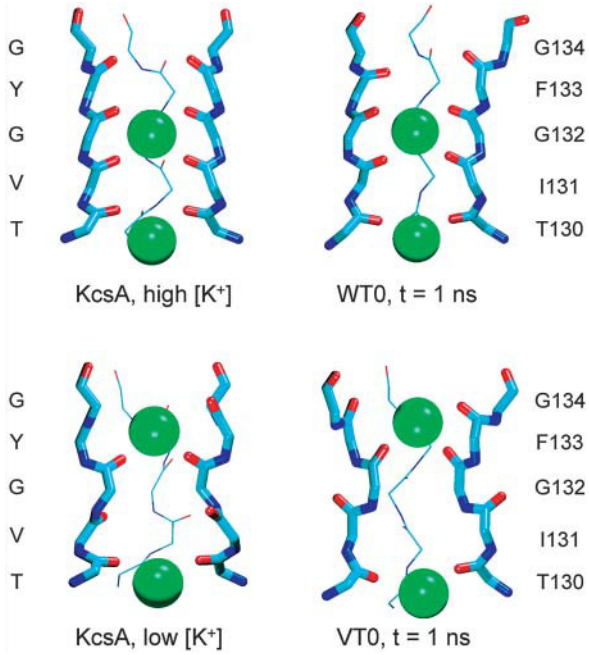

FIGURE 7 Comparison of the two x-ray structures of the KcsA filter region with snapshots from the WT0 and VT0 simulations. In each case just two subunits (and two K^+ ions) are shown. The structures shown are for KcsA at high [K^+] (PDB code 1K4C); Kir6.2 simulation WT0 at 1 ns; KcsA at low [K^+] (PDB code 1K4D); and Kir6.2 simulation VT0 (i.e., the lowest conductance mutant) at 1 ns.

ular, the backbone carbonyls of I131 have flipped so as to be no longer directed toward the pore. This has the effect of moving the carbonyl oxygens of G132 a little further in toward the filter, thus narrowing the pore in this region. This shows significant similarities to the conformation of the KcsA filter in the presence of low [K^+] although the extent of flipping of the V76 carbonyls (equivalent to I131 of Kir6.2) is somewhat less pronounced in KcsA.

We can attempt to relate these distortions in the filter of the Kir models to changes in patterns of H-bonding. Thus, at $t = 1$ ns, in the WT0 model the backbone carbonyl of E126 is H-bonded to the amides of G132 and F133, and the carbonyl of V127 is able to H-bond to the NH of I131. These interactions help to orient the NH groups of the filter away from the pore and hence prevent flipping of the peptide groups of the filter. In contrast, in model VT0, it seems that the O-atom of the side chain of T127 H-bonds to W26. This prevents the backbone carbonyl of T127 from H-bonding to the amide of I131, and instead the amide of I131 H-bonds to the carbonyl of E126. This, in turn, frees the amides of G132 and F133, allowing these residues greater flexibility; and so flipping of the peptide groups is more likely to occur.

Functional consequences

Let us examine the possible functional consequences of such enhanced filter flexibility, again focusing on the comparison between simulations WT0 and VT0. One simple way in which to do this is to evaluate pore radius profiles (Smart et al., 1993, 1996) for the filter. In Fig. 8 we compare: (*a*) the pore radius profiles of Kir6.2 WT0 over a 100-ps period at $t \sim 1$ ns with that of high [K^+] KcsA; and (*b*) the profiles of Kir6.2 VT0 over a 100-ps period at $t \sim 1$ ns and low [K^+] KcsA. The WT0 and high [K^+] KcsA profiles are very similar, with the binding site radii approximately equal to that of a K^+ ion (0.133 nm). In contrast, both the low [K^+] and the VT0 profiles show a significant degree of narrowing (to radius ~0.06 nm) of the pore in the region where S2 was in the other structures. This would be expected to present a considerable barrier to permeation through the filter. The resemblance between the filter radius profiles for VT0 and low [K^+] KcsA is quite striking. Of course, this is just for a single conformation from the VT0 simulation. However, examination of filter radius profiles as a function of time along the VT0 trajectory show similar behavior for the period during which I131 is flipped.

Motion of ions and water through the filter region can be simply represented by plotting the trajectories projected onto the pore (i.e., *z*-) axis versus time. Comparing trajectories for different simulations provides insight into how changes in filter structures caused by mutations and/or presence of water molecules behind the filter region may affect the process of ion permeation, at least on an ns-timescale. In the WT simulations ions move rapidly in a concerted fashion from a 01010 to a 00101 configuration. This is shown for WT3 in

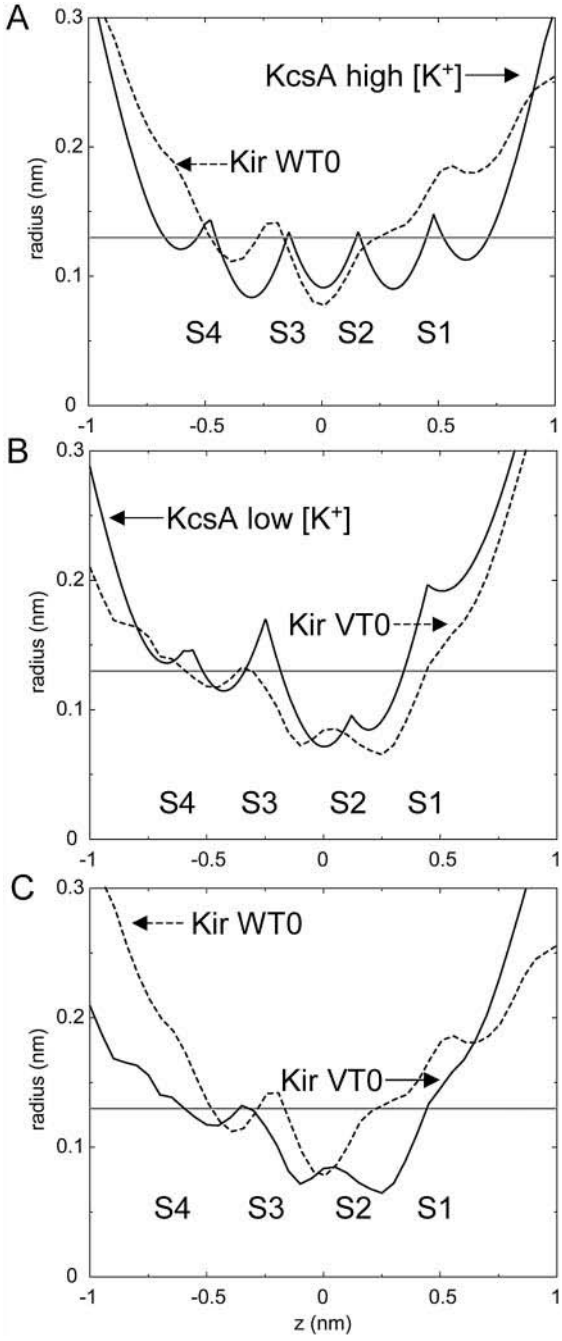

FIGURE 8 Pore radius profiles for the filter regions of: (*A*) KcsA at high [K^+] (*solid line*) versus Kir6.2 simulation WT0 at ~1 ns (*broken line*, average of profiles at 10-ps intervals from 0.95 to 1.05 ns); and (*B*) KcsA at low [K^+] (*solid line*) versus Kir6.2 mutant simulation VT0 (*broken line*, average of profiles at 10-ps intervals from 0.95 to 1.05 ns) at ~1 ns. The horizontal gray line represents the radius of a K^+ ion. In (*C*) the Kir6.2 WT0 and VT0 profiles at ~1 ns are redisplayed to facilitate direct comparison.

Fig. 9 *A* where this concerted motion occurs after ~50 ps of simulation time. In the V127T simulations we see a different picture, whereby the ions are able to move in a nonconcerted fashion. In VT0 (Fig. 9 *B*) the ion in site S3 moves down into site S4 after ~200 ps. However, the concerted motions of

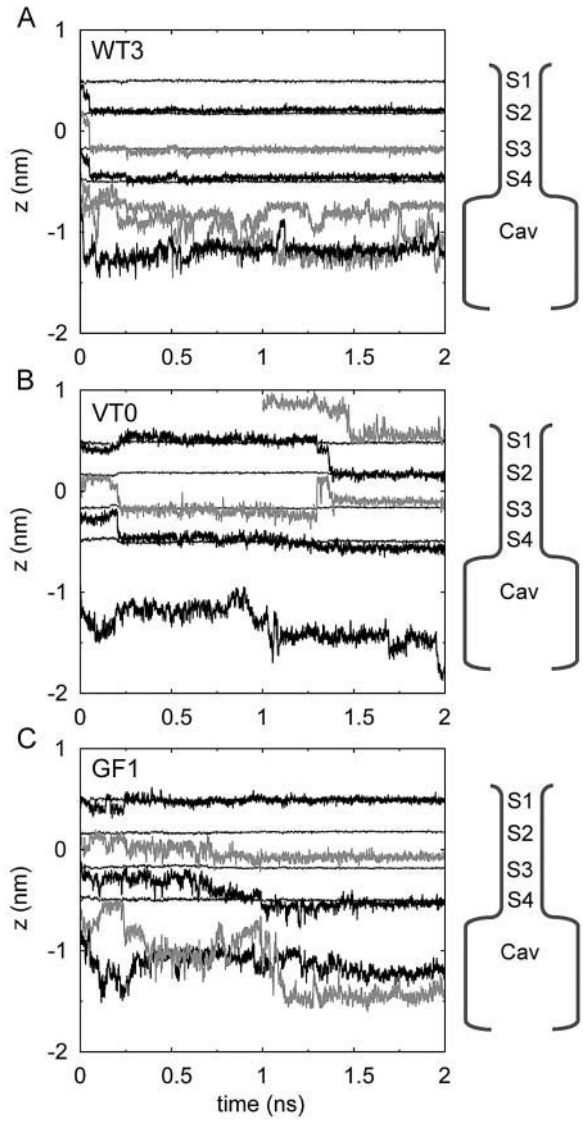

FIGURE 9 Trajectories, projected onto the filter (z-) axis, of K^+ ions (*black lines*) and selected water molecules (*gray lines*) within the channel. The four binding sites S1–S4 are shown as thin black lines. The diagram to the right of each graph is a schematic of the filter and cavity of the channel. Results are shown for simulations: (*A*) WT3; (*B*) VT0; and (*C*) GF1.

the two ions are hampered by the altered structure of the selectivity filter. The carbonyl oxygens of I131 flip outwards to point away from the pore center (see above). This pinches the top of the filter tighter, making it impossible for the ion in site S1 to move to S2. At the same time, as half of the oxygens which make up site 2 are oriented away from the pore it means that this site would be unable to fully coordinate a K^+ ion. This results in a 01001 configuration of the filter which is maintained for over a nanosecond. After this the carbonyl oxygens of I131 move back toward the pore and the upper ion is then able to move from S1 into S2. Thus, by the end of the simulation we have observed the same overall ion transition as in the WT, yet via a slightly different mechanism, arising from the increased probability of the I131 carbonyls being oriented away from the pore. The translocation process would appear to take longer in the V127T mutant than the WT as a result of this different mechanism, whereby there is an increased probability of the filter being in this low permeability conformation. This nonconcerted motion of ions is also seen in the VT1 and VT3 simulations, although in the latter case the selectivity filter becomes very distorted such that the binding sites become hard to define.

The G135F and M137C mutations, which cause intermediate conductance between WT and V127T levels, are also able to exhibit some nonconcerted ion motion. The GF0 simulation behaves much as the WT simulations do, with a clear concerted transition of ions from 01010 to 00101 occurring very rapidly at the start of the simulation. For MC0 the transition is again clear and concerted, but occurs after ~700 ps of simulation rather than at the start. However, in the GF1 and MC1 simulations, the I131 carbonyl flip is observed which prevents the transition of an ion from S1 to S2, and for GF1 the configuration is to 01001 after 2 ns (Fig. 9 *C*). For MC1 the filter distorts, allowing more waters in the top, and these are able to coordinate the K^+ ion as it moves into S2. Interestingly, in the GF3 and MC3 simulations the motion is concerted, although not as rapid as in the WT3 simulations, with ions appearing to move more gradually from one site to the next over ~200 ps rather than moving via a sudden jump within a few picoseconds.

We can make a rough estimate of the effects of these distortions on the predicted conductance of the channel. If, from the data in Fig. 5, we estimate from the percentage time in the VT simulations that the filter adopts a distorted/flipped conformation, we arrive at a figure of ~54% of the time. If we assume that this conformation corresponds to a functionally closed filter, then on the timescale of patch clamp recording we would predict the single-channel conductance of V127T to be ~50% of that of the WT channel. The experimental data (Proks et al., 2001) suggests that V127T single-channel conductance is ~40% that of the WT. Given that the current duration of these simulations still raises issues of incomplete statistical sampling, this is a remarkable correspondence between simulation and experiment.

DISCUSSION

Critique of methodology

Kir6.2 channel models

With respect to the WT model there are two possible limitations of the procedures we have adopted: 1), the input sequence alignment of KcsA and Kir6.2; and 2), the use of the lower resolution KcsA structure as the template. With respect to the sequence alignment, we note that some other investigators (e.g., Minor et al., 1999) have used an alignment that differs from ours in the M2 helix region and

have suggested that KcsA and Kir channels may not share the same three-dimensional fold in terms of the packing of the M1 and M2 helices. However, more recently, Durell and Guy (2001) have identified a bacterial homolog of mammalian Kir channels which provides an unambiguous alignment between the KcsA and Kir sequences. Furthermore, the alignment used here and by Capener et al. (2000) preserves the conserved glycine residue (G99 in KcsA) in KcsA and MthK that has been suggested to play a key role in gating of K channels (Jiang et al., 2002b). We have also compared homology models of Kir6.2 based on the two alternative sequence alignments relative to KcsA by 10-ns MD simulations of both models embedded in a membrane-mimetic octane slab (Capener and Sansom, unpublished results; Sansom et al., 2002). The more KcsA-like model (i.e., the one used in this article and our earlier publications) revealed significantly less structural drift over the course of the simulation. Experimental studies, including cysteine-scanning mutagenesis studies by Loussouarn et al. (2001) and the creation of a *functional* chimeric K channel by inserting the M1-P-F-M2 region of KcsA within the cytoplasmic N- and C-terminal domains of Kir2.1 (Lu et al., 2001), also support the underlying assumption that Kir and KcsA share the same TM domain fold.

With respect to the use of the lower resolution structure of KcsA as a template we suspect that, given the errors inherent in homology modeling, the changes between the 3.2-Å and 2-Å resolution structures would not significantly alter the quality of the Kir homology models. Furthermore, in this paper we are focusing on events at the selectivity filter: preliminary comparison of KcsA simulations based on the 3.2-Å structure (Shrivastava and Sansom, 2000) and the 2-Å structure (Domene et al., unpublished data) suggest similar behavior of water, ions, and protein on a nanosecond timescale. However, it will be important in future studies to use Kir6.2 models based on the higher resolution x-ray structure of KcsA.

It may be argued that homology models are not sufficiently accurate to form the basis of meaningful simulations. For any given case it is difficult to give a definitive answer until the structure of the protein being modeled is solved. However, we would suggest that our previous studies of Kir6.2, based on such simulations (Capener et al., 2000; Capener and Sansom, 2002), indicate that meaningful conclusions may be derived. For a somewhat different protein, comparative simulations of aquaporin-1 based on a homology model (itself based on the bacterial protein GlpF; see Fu et al., 2000) versus simulations based on the x-ray structure of Aqp1 (Sui et al., 2001) yielded strong similarities in terms of the behavior of water within the channel pore. In particular, the functionally important reversal of water dipole orientation midway along the pore first seen by De Groot and Grubmuller (2001) and by Tajkhorshid et al. (2002) has also been seen by us in simulations based on a low resolution (~4.5-Å) structure, on a homology model, and on the 2.2-Å resolution x-ray structure (Law and Sansom, unpublished data). This supports our suggestion that functionally relevant conclusions may be derived from simulations based on homology models.

The other main limitation of our models is the absence of the substantial N- and C-terminal domains of Kir6.2, that are known to contribute to ATP-dependent gating of the channel (Tucker et al., 1998). In the absence of three-dimensional structures for these domains (57 residues for the N-terminal, and 215 for the C-terminal, domain) there is little else one can do. However, we should remember that binding of ligands to these domains may be capable of allosteric regulation of changes in the filter conformation.

Simulations

There are two main technical limitations of the current simulations: 1), the duration (2 ns) of each simulation; and 2), the use of an, albeit long, cutoff for long-range electrostatic interactions rather than, for example, partical-mesh Ewald (Darden et al., 1993). We are reasonably confident that neither of these acknowledged approximations will have significantly distorted the outcome of our studies. In previous simulations of Kir6.2 and of KcsA we have seen that the filter can change on a nanosecond timescale. Of course, longer simulations would have yielded better sampling for a given starting configuration, but we elected to explore multiple starting configurations in terms of different initial positions of water molecules around the filter and different mutants. We would note that the total duration of the simulations in this study is ~27 ns.

With respect to use of a cutoff rather than PME we accept that the former is an approximation. Our justification for this is that, in previous simulations of WT Kir6.2 in which we examined the effects of changes in simulation conditions, we found no significant differences in the behavior of the filter and its ions between cutoff and PME simulations (Capener and Sansom, 2002).

Biological implications

Permeation mechanism

In the WT models during most of the simulation and in KcsA at high $[K^+]$ the filter carbonyl oxygens are pointing toward the pore to coordinate permeating potassium ions. It has been reported in numerous simulation studies of KcsA (Bernèche and Roux, 2000, 2001; Shrivastava et al., 2002; Guidoni et al., 2000) and Kir6.2 (Capener and Sansom, 2002) that these carbonyls may transiently move away from the pore as ions translocate from one site to the next, to prevent steric hindrance, i.e., to smooth the permeation energy landscape. In addition, x-ray crystallography demonstrated how, under low $[K^+]$ conditions, the carbonyls of KcsA are also able to

move away from the pore, thus avoiding repulsion of negative charges when no cation is present. This is a somewhat larger change in conformation than that occurring during permeation. However, if the carbonyl oxygens are for some reason trapped in the low [K^+] conformation, it is expected to prevent ions from moving through the filter, as a K^+ ion is unlikely to move from a site at which it is fully coordinated to one where its effective coordination shell would be incomplete. Only when the carbonyl oxygens move back toward the pore can the ion move into the adjacent site. On this basis, we would suggest that the highly distorted conformation of the filter, which we have shown to be close to that of low [K^+] KcsA, corresponds to a transiently closed conformation of the channel.

Effects of mutations around the filter

Physiological data shows that V127T is the most disruptive of the mutations, with the G135F and M137C having a lesser effect on conductance levels (and fast gating kinetics). This trend is reflected in the simulations. In particular, we are able to identify differences in the conformations of the filter-lining carbonyls caused by mutations in the P + F region. We see that the V127T mutant appears to stabilize (i.e., shift the equilibrium toward) a conformation in which the I131 carbonyls point away from the pore, thus preventing ion motion for the reason outlined above.

We also note that effects of mutations within the filter region did not appear to be directly coupled to the behavior of the TM helices; rather, any differences in the motions of M1 and M2 between the various simulations appear to arise from the slight deviations involved within the homology modeling procedure. It therefore remains difficult to envisage how allosteric effects of ATP-binding may be conveyed to the filter; further studies in this area are clearly needed.

Waters embedded in the filter

Preliminary results from simulations based on models of the mutants hinted at an important role for water molecules buried between the P-helix and filter regions in affecting conformational dynamics of the filter region. High-resolution x-ray crystal structures of KcsA purified in low (3-mM) and high (200-mM) K^+ concentrations reveal different numbers (one versus three per subunit) of water molecules localized in this region. In the high [K^+] structure of KcsA, one water molecule per subunit is associated with this region, located behind G79 where it is able to form a hydrogen bond to the amide nitrogen. In the low [K^+] structure, there are three water molecules per subunit buried in this protein region. One is hydrogen-bonded to the V76 carbonyl, which is pointing away from the pore (unlike in the high [K^+] structure). This is also H-bonded to the second water molecule, which is in turn H-bonded to the amide nitrogen of G77 on the adjacent subunit. The third water molecule is located approximately at the position of the water in the high [K^+] structure, but a little further away from the pore such that it predominately mediates the bond between D80 and E71. In Kir6.2 the corresponding waters (in the three waters/subunit simulations) form H-bonds to the carbonyl oxygens of the I131 residues and the amide hydrogens of G132 and G134. In the WT simulation (WT3) these H-bonds exist for ~50% of the time overall. In contrast, in simulation VT3, these H-bonds are formed for a greater proportion of the total simulation time, with those to G134 predominating.

We show that, in the WT and mutant models studied, the presence of water molecules behind the selectivity filter is able to modulate the motions of the filter backbone, allowing additional regions of conformational (Φ,Ψ) space to be sampled. The presence of just one water per subunit seems to have a more dramatic effect than when three are present, by providing a restricted alternative conformation to that which is seen when there are no waters present behind the filter. The filter can become trapped in this conformation. Presence of three waters per subunit appears to saturate the region, making both conformations accessible and interchangeable; this results in more of the WT conformation being observed.

Comparison with KcsA

The two KcsA high resolution structures reveal that a certain amount of conformational flexibility is allowed within the selectivity filter region. The two distinct conformations seen under high and low [K^+] conditions are suggested to correspond to a conducting and a nonconducting conformation of the filter (Zhou et al., 2001). This is in agreement to our observations on ion permeation, i.e., that when a highly distorted (similar to low K) conformation of the filter occurs, the orientation of carbonyls away from the pore region erects a barrier on the ion permeation energy profile and prevents motion of ions from one site to the next.

In this study we found it instructive to compare the filter structures we observe for WT Kir6.2 and the mutant Kirs back to the KcsA structures. In particular, our simulation snapshots of the filter structure of the WT Kir6.2 remained close to the filter structure found for KcsA crystallized under high K^+ concentrations, whereas filter structure of the low-conductance mutant V127T in simulations was found to correspond much more closely to the structure of KcsA crystallized under low [K^+] conditions. Thus the V127T mutation alters the preferred conformation of the Kir filter from the WT carbonyl-in orientation to the nonconducting carbonyl-out orientation. By shifting this equilibrium toward a nonconducting state of the filter, the V127T mutation is able to reduce the K^+ conductance as measured on a millisecond timescale.

In summary, our results suggest that simulations based on homology models of wild-type and mutant Kir6.2 channels can provide insights into possible changes in equilibrium filter conformation that underlie changes in single-channel

conductance. It is of interest that these mutations also perturb the fast gating kinetics of Kir6.2 channels. It is possible that the changes in filter conformation described in this study may also be related to fast gating. However, methods capable of exploring much longer timescales ($\sim$10 μs) will be needed before fast gating can be explored directly by simulation.

We are grateful to O.S.C. for computer time. C.E.C. is a BBSRC research student. Our thanks to members of M.S.P.S.'s research group and to Declan Doyle for helpful discussions.

This work was funded by grants from The Wellcome Trust (to M.S.P.S. and to F.M.A.).

REFERENCES

Adcock, C., G. R. Smith, and M. S. P. Sansom. 1998. Electrostatics and the selectivity of ligand-gated ion channels. *Biophys. J.* 75:1211–1222.

Åqvist, J., and V. Luzhkov. 2000. Ion permeation mechanism of the potassium channel. *Nature*. 404:881–884.

Ashcroft, F. M., M. Kakei, and R. P. Kelly. 1989. Rubidium and sodium permeability of the ATP-sensitive K channel in single rat pancreatic beta-cells. *J. Physiol.* 408:413–430.

Berendsen, H. J. C., J. P. M. Postma, W. F. van Gunsteren, A. DiNola, and J. R. Haak. 1984. Molecular dynamics with coupling to an external bath. *J. Chem. Phys.* 81:3684–3690.

Berger, O., O. Edholm, and F. Jahnig. 1997. Molecular dynamics simulations of a fluid bilayer of dipalmitoylphosphatidycholine at full hydration, constant pressure and constant temperature. *Biophys. J.* 72: 2002–2013.

Bernèche, S., and B. Roux. 2000. Molecular dynamics of the KcsA K^+ channel in a bilayer membrane. *Biophys. J.* 78:2900–2917.

Bernèche, S., and B. Roux. 2001. Energetics of ion conduction through the K^+ channel. *Nature*. 414:73–77.

Biggin, P. C., T. Roosild, and S. Choe. 2000. Potassium channel structure: domain by domain. *Curr. Opin. Struct. Biol.* 10:456–461.

Capener, C. E., and M. S. P. Sansom. 2002. MD Simulations of a K channel model—sensitivity to changes in ions, waters and membrane environment. *J. Phys. Chem. B.* 106:4543–4551.

Capener, C. E., I. H. Shrivastava, K. M. Ranatunga, L. R. Forrest, G. R. Smith, and M. S. P. Sansom. 2000. Homology modelling and molecular dynamics simulation studies of an inward rectifier potassium channel. *Biophys. J.* 78:2929–2942.

Choe, H., H. Sackin, and L. G. Palmer. 2000. Permeation properties of inward-rectifier potassium channels and their molecular determinants. *J. Gen. Physiol.* 115:391–404.

Darden, T., D. York, and L. Pedersen. 1993. Particle mesh Ewald—an N.log(N) method for Ewald sums in large systems. *J. Chem. Phys.* 98:10089–10092.

Davis, M. E., J. D. Madura, B. A. Luty, and J. A. McCammon. 1991. Electrostatics and diffusion of molecules in solution: simulations with the University of Houston Brownian dynamics program. *Comput. Phys. Comm.* 62:187–197.

De Groot, B. L., and H. Grubmuller. 2001. Water permeation across biological membranes: mechanism and dynamics of aquaporin-1 and GlpF. *Science*. 294:2353–2357.

Doyle, D. A., J. M. Cabral, R. A. Pfuetzner, A. Kuo, J. M. Gulbis, S. L. Cohen, B. T. Cahit, and R. MacKinnon. 1998. The structure of the potassium channel: molecular basis of K^+ conduction and selectivity. *Science*. 280:69–77.

Durell, S. R., and H. R. Guy. 2001. A putative prokaryote member of the Kir family of potassium channels. *BioMed. Central Evol. Biol.* 1:14.

Fu, D., A. Libson, L. J. W. Miercke, C. Weitzman, P. Nollert, J. Krucinski, and R. M. Stroud. 2000. Structure of a glycerol-conducting channel and the basis of its selectivity. *Science*. 290:481–486.

Guidoni, L., V. Torre, and P. Carloni. 2000. Water and potassium dynamics in the KcsA K^+ channel. *FEBS Lett.* 477:37–42.

Hermans, J., H. J. C. Berendsen, W. F. van Gunsteren, and J. P. M. Postma. 1984. A consistent empirical potential for water-protein interactions. *Biopolymers*. 23:1513–1518.

Hess, B., H. Bekker, H. J. C. Berendsen, and J. G. E. M. Fraaije. 1997. LINCS: a linear constraint solver for molecular simulations. *J. Comp. Chem.* 18:1463–1472.

Hille, B. 2001. Ionic Channels of Excitable Membranes. Sinauer Associates Inc., Sunderland, Massachusetts.

Humphrey, W., A. Dalke, and K. Schulten. 1996. VMD—Visual Molecular Dynamics. *J. Mol. Graph.* 14:33–38.

Jiang, Y., A. Lee, J. Chen, M. Cadene, B. T. Chait, and R. MacKinnon. 2002a. Crystal structure and mechanism of a calcium-gated potassium channel. *Nature*. 417:515–522.

Jiang, Y., A. Lee, J. Chen, M. Cadene, B. T. Chait, and R. MacKinnon. 2002b. The open pore conformation of potassium channels. *Nature*. 417:523–526.

Killian, J. A., and G. von Heijne. 2000. How proteins adapt to a membrane-water interface. *Trends Biochem. Sci.* 25:429–434.

Kubo, Y., and Y. Murata. 2001. Control of rectification and permeation by two distinct sites after the second transmembrane region in Kir2.1 K+ channel. *J. Physiol.* 531:645–660.

Loussouarn, G., L. R. Phillips, R. Masia, T. Rose, and C. G. Nichols. 2001. Flexibility of the Kir6.2 inward rectifier K^+ channel pore. *Proc. Natl. Acad. Sci. USA*. 98:4227–4232.

Lu, T., B. Nguyen, X. Zhang, and J. Yang. 1999. Architecture of a K+ channel inner pore revealed by stoichiometric covalent modification. *Neuron*. 22:571–580.

Lu, Z., A. M. Klem, and Y. Ramu. 2001. Ion conduction pore is conserved among potassium channels. *Nature*. 413:809–813.

Marrink, S. J., O. Berger, D. P. Tieleman, and F. Jahnig. 1998. Adhesion forces of lipids in a phospholipid membrane studied by molecular dynamics simulations. *Biophys. J.* 74:931–943.

Merritt, E. A., and D. J. Bacon. 1997. Raster3D: photorealistic molecular graphics. *Methods Enzymol.* 277:505–524.

Minor, D. L., S. J. Masseling, Y. N. Jan, and L. Y. Jan. 1999. Transmembrane structure of an inwardly rectifying potassium channel. *Cell*. 96:879–891.

Morais-Cabral, J. H., Y. Zhou, and R. MacKinnon. 2001. Energetic optimization of ion conduction by the K^+ selectivity filter. *Nature*. 414:37–42.

Morris, A. L., M. W. MacArthur, E. G. Hutchinson, and J. M. Thornton. 1992. Stereochemical quality of protein structure coordinates. *Prot. Struct. Funct. Genet.* 12:345–364.

Proks, P., C. E. Capener, P. Jones, and F. Ashcroft. 2001. Mutations within the P-loop of Kir6.2 modulate the intraburst kinetics of the ATP-sensitive potassium channel. *J. Gen. Physiol.* 118:341–353.

Reimann, F., and F. M. Ashcroft. 1999. Inwardly rectifying potassium channels. *Curr. Opin. Cell Biol.* 11:503–508.

Sali, A., and T. L. Blundell. 1993. Comparative protein modeling by satisfaction of spatial restraints. *J. Mol. Biol.* 234:779–815.

Sansom, M. S. P., I. H. Shrivastava, J. N. Bright, J. Tate, C. E. Capener, and P. C. Biggin. 2002. Potassium channels: structures, models, simulations. *Biochim. Biophys. Acta*. 1565:294–307.

Schiffer, M., C. H. Chang, and F. J. Stevens. 1992. The functions of tryptophan residues in membrane proteins. *Prot. Eng.* 5:213–214.

Shrivastava, I. H., and M. S. P. Sansom. 2000. Simulations of ion permeation through a potassium channel: molecular dynamics of KcsA in a phospholipid bilayer. *Biophys. J.* 78:557–570.

Shrivastava, I. H., D. P. Tieleman, P. C. Biggin, and M. S. P. Sansom. 2002. K^+ vs. Na^+ ions in a K channel selectivity filter: a simulation study. *Biophys. J.* 83:633–645.

Smart, O. S., J. M. Goodfellow, and B. A. Wallace. 1993. The pore dimensions of gramicidin A. *Biophys. J.* 65:2455–2460.

Smart, O. S., J. G. Neduvelil, X. Wang, B. A. Wallace, and M. S. P. Sansom. 1996. HOLE: a program for the analysis of the pore dimensions of ion channel structural models. *J. Mol. Graph.* 14:354–360.

Straatsma, T. P., and H. J. C. Berendsen. 1988. Free-energy of ionic hydration—analysis of a thermodynamic integration technique to evaluate free-energy differences by molecular-dynamics simulations. *J. Chem. Phys.* 89:5876–5886.

Sui, H. X., B. G. Han, J. K. Lee, P. Walian, and B. K. Jap. 2001. Structural basis of water-specific transport through the AQP1 water channel. *Nature.* 414:872–878.

Tajkhorshid, E., P. Nollert, M. O. Jensen, L. J. W. Miercke, J. O'Connell, R. M. Stroud, and K. Schulten. 2002. Control of the selectivity of the aquaporin water channel family by global orientational tuning. *Science.* 296:525–530.

Thompson, G. A., M. L. Leyland, I. Ashmole, M. J. Sutcliffe, and P. R. Stanfield. 2000. Residues beyond the selectivity filter of the K^+ channel Kir2.1 regulate permeation and block by external Rb^+ and Cs^+. *J. Physiol.* 526:231–240.

Tieleman, D. P., and H. J. C. Berendsen. 1996. Molecular dynamics simulations of a fully hydrated dipalmitoylphosphatidycholine bilayer with different macroscopic boundary conditions and parameters. *J. Chem. Phys.* 105:4871–4880.

Tieleman, D. P., H. J. C. Berendsen, and M. S. P. Sansom. 1999. An alamethicin channel in a lipid bilayer: molecular dynamics simulations. *Biophys. J.* 76:1757–1769.

Tucker, S. J., F. M. Gribble, P. Proks, S. Trapp, T. J. Ryder, T. Haug, F. Reimann, and F. M. Ashcroft. 1998. Molecular determinants of K_{ATP} channel inhibition by ATP. *EMBO J.* 17:3290–3296.

Yau, W. M., W. C. Wimley, K. Gawrisch, and S. H. White. 1998. The preference of tryptophan for membrane interfaces. *Biochemistry.* 37:14713–14718.

Zhou, Y., J. H. Morais-Cabral, A. Kaufman, and R. MacKinnon. 2001. Chemistry of ion coordination and hydration revealed by a K^+ channel-Fab complex at 2.0 Å resolution. *Nature.* 414:43–48.